Coherence Length and Vibrations of the Coherence Beamline I13 at the Diamond Light Source

2017 J. Phys.: Conf. Ser. 849 012048

(http://iopscience.iop.org/1742-6596/849/1/012048)

Coherence Length and Vibrations of the Coherence Beamline I13 at the Diamond Light Source

U.H. Wagner[1], A. Parson[1], C. Rau[1,2]

[1] Diamond Light Source, Chilton, Didcot, Oxon OX11 0DE
[2] Northwestern University, Chicago (IL), USA, 60611-3008

ulrich.wagner@diamond.ac.uk

Abstract. I13 is a 250 m long hard x-ray beamline for imaging and coherent diffraction at the Diamond Light Source. The beamline (6 keV to 35 keV) comprises two independent experimental endstations: one for imaging in direct space using x-ray microscopy and one for imaging in reciprocal space using coherent diffraction based imaging techniques [1]. In particular the coherence experiments pose very high demands on the performance on the beamline instrumentation, requiring extensive testing and optimisation of each component, even during the assembly phase. Various aspects like the quality of optical components, the mechanical design concept, vibrations, drifts, thermal influences and the performance of motion systems are of particular importance. In this paper we study the impact of the front-end slit size (FE slit size), which determines the horizontal source size, onto the coherence length and the detrimental impact of monochromator vibrations using in-situ x-ray metrology in conjunction with fringe visibility measurements and vibration measurements, based on centroid tracking of an x-ray pencil beam with a photon-counting detector.

1. Beamline Layout and Coherence Length adjustment via Front-end Slits

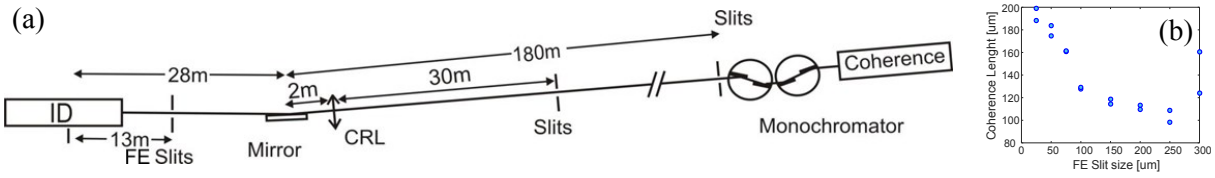

Figure 1. (a) Beamline Layout (b) Variation of the coherence length with FE slit size at 8.0 KeV.

The beamline layout is shown in figure 1(a). The three outstanding features of the beamline are: The front-end slits (FE slits), which are located close to the horizontal source point, thanks to the double mini-beta design [2], and allow to directly adjust the horizontal source size and subsequently the coherence length. Secondly all optical components are horizontally deflecting to minimise the loss of coherent flux [3], arising from the optics performance and the component's stability. Thirdly the monochromator is located close to the end-station to allow for water cooling and thus avoids the technical challenge to use a liquid nitrogen cooling system, which does not induce vibrations and drifts.

Figure 1(b) shows how opening and closing the FE slits adjusts the coherence length, which has been measured using the fringe visibility of a boron-fibre diffraction pattern [4]. In [5] details about

the measurements at I13 are given: The vertical coherence length has been found to be larger than 350 μm whilst the horizontal coherence length appears to be limited to 200 μm, even if the FE slits are closed to approximately 25 μm. This might be due to limitations within the FE slit design, in particular the slit blades, or vibrations within the horizontally deflecting beamline optics.

As shown in [3] any vibrations of the monochromator will have the most profound impact onto the beamline performance, since it is the most downstream optical component. Simply speaking a rotational vibration between the first and second crystal of the monochromator with an rms-amplitude α_{rms} at a distance $\mathrm{r_m} = 197.5$ m from the FE slits, which are opened to d_{Slit}, will lead to an increase of the apparent FWHM of the virtual source ${\mathrm{w_s}}^2 \approx {d_{Slit}}^2 + \left(2\sqrt{8\ln(2)}\,\alpha_{\mathrm{rms}}\,\mathrm{r_m}.\right)^2$. Using the van Citter-Zernicke theorem and the apparent source size one can derive the coherence length $\mathrm{l_{tc}} = \frac{\sqrt{2}\,\lambda}{\pi}\,\frac{\mathrm{r_s}}{\mathrm{w_s}}$, whereby $2\mathrm{l_{tc}}$ corresponds to the FWHM of the mutual intensity function and $\mathrm{r_s} = 201$ m is the distance from the FE slits to the boron-fiber. Vice versa, if one measures the coherence length one can derive the apparent source size and subsequently, if the FE slit size d_{Slit} is known, an upper estimate of the monochromator vibrations.

Table 1. Coherence length, apparent source size and vibrations versus FE slit size: Slit sizes beyond 100 μm have not been considered, since the Gaussian profile of the x-ray beam increasingly determines the photon-beam size rather than the FE slits for larger slit openings.

FE Slit Size d_{Slit}[μm]	25	50	75	100
Coherence Length $\mathrm{l_{tc}}$ [μm]	195	180	160	129
Apparent Source Size $\mathrm{w_s}$ [μrad(FWHM)]	77	83	93	115
Angular Vibration α_{rms} [nrad(rms)]	57	55	66	73

Table 1 is derived from figure 1(b) and shows that the monochromator vibrations vary between 57 nrad(rms) and 73 nrad(rms). The data for the fringe visibility analysis were collected over 40 seconds per point, whilst the Bragg axis control loop was switched off. The variation of the vibration- level arises most likely from the relatively short data acquisition time. Reducing the overall amplitude of vibrations, in particular transient excitations, will yield the largest benefits in increasing the horizontal coherence length, but requires more detailed in-situ spectral analysis.

2. In-situ vibration measurements using a Photon Counting Detector

It is very beneficial to study vibrations already during the assembly of the instrument using optical or mechanical metrology equipment [6] to ensure a correct design and assembly and to mitigate any glitches. Nevertheless the final and ultimate tests have to be performed using in-situ x-ray based techniques. The most simple and direct method to measure vibrations is to use an x-ray pencil beam and track the motion of its centroid with a high frame-rate and high resolution x-ray detector.

Detectors achieving a resolution of less than 1 μm tend to have lower quantum efficiency (typically around 0.44 counts/x-ray Photon) and higher noise levels (>2.2 counts(rms)), since they are detecting the x-rays indirectly via a scintillation screen and a high resolution microscope objective. Directly detecting detectors can have quantum efficiencies approaching 1.0 and are virtually noise free, but have a larger pixel size and thus less resolution. This drawback can often be compensated by better sub-pixel interpolation:

For simplicity, let us assume an x-ray pencil beam, which is precisely one pixel wide and centered between two pixels, so that it is split equally between the two pixels and the total number of counts per pixel is c_p. If the pixel size is d_P and the beam moves towards one pixel by δx, then its counts will increase to $\mathrm{c_p}(1 + 2\delta x/d_P)$ and for the other pixel, it will decrease to $c_p(1 - 2\delta x/d_P)$, thus converting position information into a difference Δc in counts between the two pixels. The position move is then given by $\delta\mathrm{x} = \Delta c\left(d_P/4c_p\right)$ and thus limited by the smallest difference Δc, which one can measure. In the case of a noise-free detector the shot-noise of the incident x-ray photon beam, will

eventually determine the smallest observable centroid movement: The shot-noise corresponds to the square-root of the number of photons hitting a pixel and with Gaussian error propagation as an approximation, one obtains $\Delta c^2 = 2c_p$. Hence the position resolution is limited by $\Delta x^2 = {d_P}^2/8c_p$.

The photon counting detectors Merlin [7] is based on the MediPix Chip, has a pixel size of 55 µm, a frame-rate just over 1.2 KHz and provides back-to-back readout, i.e. it continuously samples the impinging photon beam without any interruption due to the readout process, thus implementing a lowpass filter with a rectangular impulse response and maximized spectral resolution. An intrinsic property of a photon-counting detector is the so called pile-up, i.e. two photons arriving in such a short period of time that the pulse counting circuity cannot discriminate between them and only counts one event. This will lead to a flattening relationship between the incident number of photons and measured counts. The pile-up becomes really significant for count-rates >200 KPhotons/sec, though it can be corrected for higher count-rates until the detector starts saturating.

3. Experimental Setup

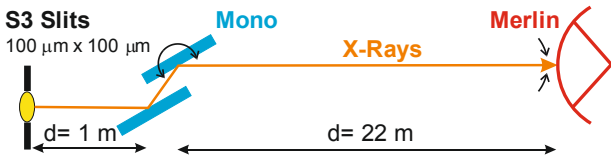

Figure 2. Setup to measure the angular vibration between the two monochromator crystals, using an x-ray energy of 9.1 KeV and Merlin, a photon-counting detector.

The experimental setup is shown in figure 2. The flux impinging onto the detector is ~200 KPhotons/Pixel/sec and the frame rate is 1.2 KHz using back to back readout. Hence there are 170 Photons/Pixel/Frame, providing a position resolution around 1.5 µm (37x sub-pixel interpolation), respectively 35 nrad pitch rotation of the monochromator crystals. In addition we could demonstrate that by illuminating a n_p pixels long row perpendicular to the measurement direction and binning the data along that row, one can improve the position sensitivity by ${n_p}^{1/2}$. The centroid positions are calculated using the EPICS ArrayDetector STAT plugin [8]. To obtain the vibration spectra a time-series with 8000 points is acquired and Fourier transformed using a Hamming-window. The statistical variation is reduced by averaging over 50 spectra. In addition the instantaneous amplitude, which is the modulus of the analytic signal and provides details about amplitude variations over time, is calculated and the different data sets are plotted in a sequence to provide an overview, how the vibrations change during the whole measurement. A Python program is used for automatizing the data acquisition and undertaking in situ data analysis.

4. Results

Table 2. Pitch vibration amplitudes of the monochromator under different operating conditions.

Bragg Axis	Chiller	Horizontal [nrad(rms)]	Vertical [nrad(rms)]
Noise Floor (Mono removed)	n.a.	39	41
Parked	Off	61	50
Parked	On	100	61
Floating	On	73	48
Normal Operation	On	166	61
Vibrating	On	280	93

The measured rms-vibration amplitudes for the monochromator under different operating conditions are summarised in table 2. To determine, if a vibration is caused by the monochromator, the monochromator is moved out of the beam and the noise floor is measured. The observed vibration level of 40 nrad(rms) corresponds well with the theoretical resolution limit of 35 nrad for the given experimental conditions and thus vibrations from other beamline-components or the machine itself are not dominant. When the monochromator is inserted, but the control system, the air supply to the

Bragg-axis and the chiller remain switched off, one observes a small increase in horizontal vibrations to 60 nrad(rms). Once the chiller is switched on this increase to 100 nrad(rms) and is mainly due to a 100Hz vibration (see inset in figure 3(a)). Switching on the air supply to the Bragg axis reduces vibrations to 73 nrad(rms), due to the reduced coupling between bearing and shaft. The most significant increase to 166 nrad(rms) is observed, when the motion control system is switched on too. Occasionally vibrations up to 280 nrad(rms) have been measured and are due to the system exciting the axis every few seconds as shown in figure 3(b).

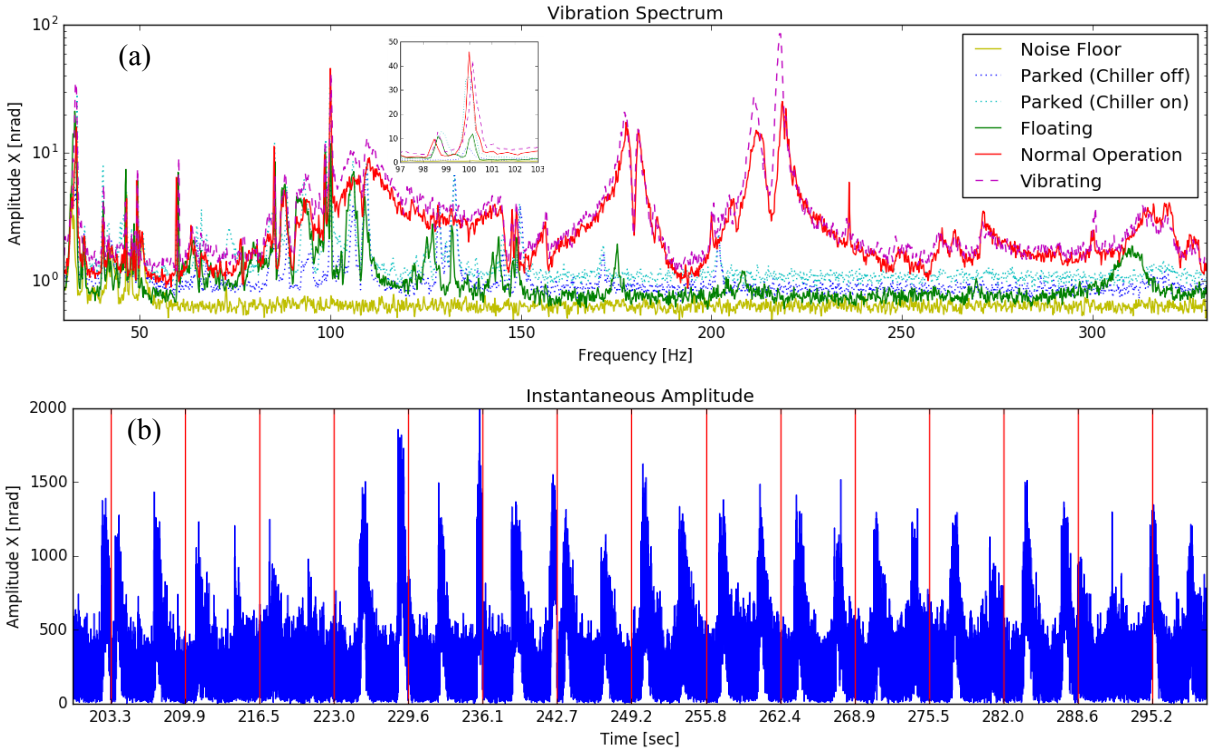

Figure 3. (a) Vibration spectra under different operating conditions. No significant vibrations are observed above 350 Hz. (b) Series of instantaneous amplitude measurements, indicating a regular excitation of the Bragg axis. The vertical lines separate the different data sets.

5. Summary

Fringe visibility measurements were used to show, how the coherence length can be adjusted with the frontend slits and an upper limit of ~200 µm was observed due to vibrations. Then vibration measurements with a resolution of 35 nrad in the spectral and time domain using an x-ray pencil beam and a photon counting detector were discussed and monochromator vibrations of ~73 nrad(rms) were measured (control system switched off), agreeing with the fringe visibility data. Finally the motion control system of the Bragg axis was identified as the main vibration source.

References

[1] C. Rau, U. Wagner, Z. Pešić, A. De Fanis 2011 *Phys. Status Solidi* **208** 2522
[2] B. Singh et al. 2009 *PAC Conference Proceedings*
[3] U.H. Wagner and C. Rau 2010 *AIP Conf. Proc.* **1234** 461
[4] V. Kohn, I. Snigireva, A. Snigirev 2000 *Pys. Rev. Lett.* **85** 2745
[5] U. H. Wagner, A. Parsons, J. Rahomaki, U. Vogt, C. Rau 2016 *AIP Conf. Proc.* **1741** 050022
[6] U. H. Wagner, S. Alcock, G. Ludbrook, J. Wiatryzk, C. Rau 2012 *AIP Conf. Proc.* **1437** 9
[7] R. Plackett, I. Horswell, E. N. Gimenez, J. Marchal et. al. 2013 *J. Instr.* **8** C01038
[8] M. L. Rivers 2010 *AIP Conf. Proc.* **1234** 51